Journal of Non-Crystalline Solids 552 (2021) 120435

Contents lists available at ScienceDirect

Journal of Non-Crystalline Solids

journal homepage: www.elsevier.com/locate/jnoncrysol

Effects of the amphoteric behavior of Al_2O_3 on the structure and properties of $CaO–SiO_2–Al_2O_3$ melts by molecular dynamics

Yang Chen, Weijie Pan, Boran Jia, Qiangqiang Wang, Xubin Zhang, Qian Wang, Shengping He*

College of Materials Science and Engineering, and Chongqing Key Laboratory of Vanadium–Titanium Metallurgy and Advanced Materials, Chongqing University, Chongqing 400044, China

ARTICLE INFO

Keywords:
$CaO–SiO_2–Al_2O_3$ melt
Amphoteric oxide
Molecular dynamics simulation
Slag structure

ABSTRACT

Amphoteric oxide Al_2O_3 is generally considered to be acidic or alkaline in different environment. The effects of Al_2O_3 on the structure and dynamic property of $CaO–SiO_2–Al_2O_3$ melt were investigated by MD simulation in this work. The results showed that as the content of Al_2O_3 increased, the contents of the tri-coordinate O and high-coordinate Al increased to balancing charge. When the basicity reaches 1, the viscosity of the melt increases with the addition of Al_2O_3 and reaches a maximum at 26 mol% of Al_2O_3. The higher concentration of Al_2O_3 leads to the relative deficiency of Ca atoms and the increase of tri-coordinate O and five-coordinate Al content, instability of the structure, and increase in D_{Al} and D_O. Al_2O_3 is considered to be acidic and forms network structures in the environment with sufficient alkaline cation. In contrast, Al_2O_3 becomes alkaline with insufficient basic cations environment, thus providing Oxygen atoms and balancing charge.

1. Introduction

$CaO-SiO_2-Al_2O_3$ is an important ternary slag system in the field of metallurgy. Al_2O_3 is a typical amphoteric oxide, showing different acidity and basicity in different slag systems. In the alkaline melts, Al_2O_3 becomes acidic, and a $[AlO_4]^{5-}$ tetrahedron structure forms between Al and O through the covalent bond Al–O, resulting in a three-dimensional network structure, which acts as a network-forming agent. In the acid melt, Al_2O_3 becomes alkaline, and the ionic bond formed between Al and anion to act as a network modifier. Presently, there are few reports on the effects of melt composition on the amphoteric behavior of Al_2O_3.

Investigations on the melt structure of the $CaO–SiO_2–Al_2O_3$ ternary system have shown that the network framework is composed of $[SiO4]^{4-}$ tetrahedron structure and a $[AlO_4]^{5-}$ tetrahedron structure, and the $[AlO_4]^{5-}$tetrahedron structure isn't as stable as the $[SiO4]^{4-}$ tetrahedron structure [1,2]. There are multiple distribution states of O in the melt, including bridging oxygen (O_b), non-bridged oxygen (O_{nb}), tri-coordinate oxygen (O_t), and free oxygen (O_f), and they are in dynamic equilibrium. Researches on the $Na_2O–Al_2O_3–SiO_2$ ternary system indicate that the role of Al_2O_3 depends on the relationship between the amount of Na and Al. When $N_{Na}/N_{Al} > 1$, Al_2O_3 becomes acidic and the $[AlO_4]^{5-}$ tetrahedron structure is formed. One of the oxygen atoms in the $[AlO_4]^{5-}$ tetrahedron structure is provided by Na_2O but it is no longer a non-bridged oxygen, and the excess negative charge of $[AlO_4]^{5-}$ is offset by Na^+ ions to achieve charge balance. When $N_{Na}/N_{Al} < 1$, a proportion of Al_2O_3 in the melt becomes alkaline, which acts as a network modifier. Al connects to six O atoms to form a $[AlO_6]$ structure. The Al–O bond becomes an ionic bond. Zheng et al [3] investigated the microstructure of calcium aluminum silicate melts with different Al/Si ratios using molecular dynamics (MD) simulation. The results showed that the acid–base boundary of Al in the melts was attained when the CaO/Al_2O_3 mole ratio was 1. The viscosity of the melts was dependent not only on the degree of polymerization of the system but also on the strength of the interaction between the particles. The research by Stebbins [5] showed the presence of three coordinated states of Al in the melt, including four-coordinate, five-coordinate, and six-coordinate Al. Among them, the four-coordinate Al, which forms the $[AlO_4]^{5-}$ tetrahedron structure, was considered to be acidic and existed as a network-forming agent, whereas the five-coordinate and six-coordinate Al served as network modifiers. And at appropriate levels of network modifiers in the melt, Al is more likely to form a $[AlO_4]^{5-}$ tetrahedron structure that participates in network formation.

Therefore, given the different acidity and basicity of the amphoteric oxide Al_2O_3, MD simulations were used in the present work to study the structures and dynamic properties of $CaO–SiO_2–Al_2O_3$ slag system. Specifically, the effect of the amphoteric nature of Al_2O_3 on the structure and properties of the ternary system were evaluated.

* Corresponding author.
E-mail address: heshp@cqu.edu.cn (S. He).

https://doi.org/10.1016/j.jnoncrysol.2020.120435
Received 9 July 2020; Received in revised form 12 September 2020; Accepted 14 September 2020

Table 1
Born–Mayer–Higgins potential parameters for atomic pairs in CaO–SiO_2–Al_2O_3 melt.

Atom1	Atom2	A_{ij}(eV)	B_{ij}(1/Å)	C_{ij}(eV•Å^6)
Ca	Ca	329051.60	6.25	4.33
Ca	Si	26674.68	6.25	0
Ca	Al	36918.57	6.25	0
Ca	O	717827.00	6.06	8.67
Si	Si	2162.39	6.25	0
Si	Al	2994.10	6.25	0
Si	O	62794.37	6.06	0
Al	Al	4142.15	6.25	0
Al	O	86057.58	6.06	0
O	O	1497049.00	5.88	17.34

2. Materials and methods

2.1. MD simulation

In the MD simulation of aluminosilicate slag, the selection of an appropriate potential function and its corresponding parameters is key to a successful simulation. The Born–Mayer–Higgins (BMH) potential function [6] is commonly applied to describe the interaction between particles in a silicate melt and was thus applied herein:

$$U_{ij}(r) = \frac{q_i q_j}{r_{ij}} + A_{ij}\exp(-B_{ij} r) - \frac{C_{ij}}{r_{ij}^6}, \quad (1)$$

where $U_{ij}(r)$ represents the potential between atoms i and j; q_i and q_j represent the amounts of charge carried by the atoms; r_{ij} represents the distance between the atoms; A_{ij} and C_{ij} are the energy parameters for the atomic pair ij describing the repulsive forces and van der Waals forces, respectively; and B_{ij} represents the e-folding length characterizing the radically symmetric decay of the electron-repulsion energy between the atomic pair ij. A_{ij}, B_{ij}, and C_{ij} are variable parameters. Empirical parameters are used in this paper, as shown in Table 1 [6]. The charges of Ca, Si, Al, and O are 2, 4, 3, and −2, respectively.

Because the BMH potential energy function assumes that melts are ionic solutions in the simulation process, the simulation system should be selected within the range of the complete melting components at the corresponding temperatures. According to the phase diagram obtained from the software FactSage, molten slag samples with different Al_2O_3 concentrations were determined in the liquid phase region at 1600 °C. The CaO–SiO_2–Al_2O_3 slag samples were divided into 8 groups and the total number of atoms in each sample was set at approximately 4000. Then, the number of different atoms was based on the mole fraction. The density of each sample at 1600 °C was calculated according to the empirical formula described therein [7]. The composition, number of atoms, and density of each sample at 1600 °C are listed in Table 2.

The choice of the simulation methods and parameters used in the simulation process, such as the number of simulated molecules, algorithm for solving the equation of motion, and total calculation time, are all important to achieve effective and accurate simulation results. In the present study, 4000 atoms were randomly placed in a model box and periodic boundary conditions were applied on all sides of the model box to create an infinite system with no boundaries. The simulation was executed in the NVT ensemble, wherein the number of atoms, the volume of samples, and the temperature are constant. In terms of the algorithm, the cutoff radius for the short-range force was set to 10 Å and the cutoff diameter was shorter than the edge length of the model box. The long-range Coulomb force uses the Ewald summation method, which is 3 × 3 × 3 in the inverse space K grid. The equations for the motions of the atoms were explained by the leapfrog integration method with a time step of 1 fs. The total time length for each MD simulation was 180 ps, which corresponds to 180000 steps. At the start of the simulation, the temperature of the system was set to 4727 °C (5000 K) for 24000 steps to mix the system adequately and eliminate any potential effects of the initial state of the atoms. Then, the temperature of the melt was cooled to 1600 °C (1873 K) through 96000 steps. Finally, the system was relaxed for 60000 steps at 1600 °C to obtain structure and transport information, such as the structure image, the partial radial distribution function (RDF), and the mean square displacement (MSD).

Table 2
Composition, number of atoms, and density of CaO–SiO_2–Al_2O_3 melts at 1600 °C.

Groups	Mole fraction (%)			Number of atoms					Density(g/cm^3)
	CaO	SiO_2	Al_2O_3	Ca	Si	Al	O	total	
CSA1	47	47	6	709	709	182	2400	4000	2.6687
CSA2	45	45	10	655	655	290	2400	4000	2.6970
CSA3	43	43	14	604	604	392	2400	4000	2.7082
CSA4	41	41	18	556	556	488	2400	4000	2.7019
CSA5	39	39	22	511	511	578	2400	4000	2.6783
CSA6	37	37	26	470	470	660	2400	4000	2.6385
CSA7	35	35	30	431	431	738	2400	4000	2.5838
CSA8	33	33	34	394	394	812	2400	4000	2.5163

2.2. Viscosity calculation

The MSD can be obtained via statistical analysis of the particle motion track in the system. The relationship between MSD and time is as follows:

$$\mathrm{MSD} = \langle \Delta\bar{r}(t)^2 \rangle = \frac{1}{N}\langle \sum |r_{i(t)} - r_{i(0)}| \rangle, \quad (2)$$

where $\Delta\bar{r}$ is the average distance between adjacent data points, N is the number of particles, and $r_{i(t)}$ and $r_{i(0)}$ are the positions of particle i at time t and $t = 0$, respectively.

The relationship between the self-diffusion coefficient D of the particles in the melt and the asymptotic limit of the particle mean azimuthal shift function for a long time can be established by the Einstein relation as follows [8]:

$$D = \lim_{t\to\infty} \frac{1}{6}\frac{\mathrm{d}[\Delta\bar{r}(t)^2]}{\mathrm{d}t}. \quad (3)$$

From the self-diffusion coefficient of particles, the shear viscosity of a melt can be calculated. The commonly used relations are the Stokes–Einstein and Eying formulae [9-12]. Based on the Stokes–Einstein and Eying formulae, the relationship between self-diffusion coefficient and shear viscosity (η) of particles in melts can be deduced as follows:

$$\eta = \frac{K_B T}{D\lambda}, \quad (4)$$

where λ is the particle transition step length, K_B is Boltzmann constant, and T is absolute temperature. Researches [13-15] have shown that when $\lambda = 2R_0$, the particle transition step length is equivalent to the distance in O^{2-} that is 2.8 Å; thus, there is a good correlation between the viscosity of silicate melts and the self-diffusion coefficient of O^{2-} ions. The oxygen that connects two silicon ions in the finite tetrahedron group is defined as bridging oxygen, and the oxygen connected to silicon ions on one side is termed as non-bridging oxygen. The structure is shown in Fig. 1.

3. Structure properties

3.1. RDF and coordination number (CN) function

The RDF describes the nearest-neighbor distributions between atoms in melts and represents the average number of atomic species j that are located at a distance r to Δr from a target atomic species i. The

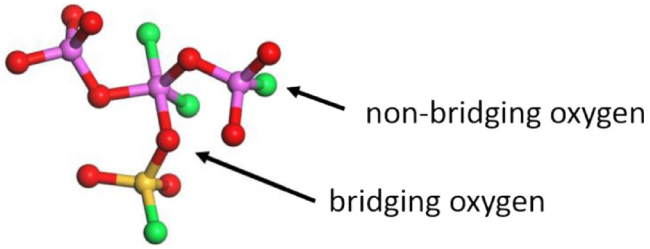

Fig. 1. Schematic of bridging and non-bridging oxygen.

equation describing the general RDF [16] is as follows:

$$g_{ij}(r) = \frac{V}{N_i N_j} \sum_j \frac{\langle n_{ij}(r - \Delta r/2, r + \Delta r/2)\rangle}{4\pi r^2 \Delta r}, \quad (5)$$

where i and j represent the atoms, V is the volume of the MD simulated box, N is the number of particles, and $n_{ij}(r - \Delta r/2, r + \Delta r/2)$ is the number of atoms j surrounding the atom i within the cutoff distance $r \pm \Delta r/2$. Integration of the corresponding partial RDF of the particles generates the average CN function, which represents the number of atoms j around atoms i within the cutoff radii. The CN function [16] is expressed as follows:

$$N_{ij}(r) = \frac{4\pi N_j}{V} \int_0^r r^2 g_{ij}(r) \mathrm{d}r. \quad (6)$$

Taking CSA5 as an example, when CaO/SiO_2 = 1 and the Al_2O_3 content is 22 mol% in the $CaO–SiO_2–Al_2O_3$ system at 1600 °C (see Table 2), the RDF and CN distribution in the melt are shown in Fig. 2. From Fig. 2(a), the average bond lengths of Si–O, Al–O, Ca–O, and O–O were 1.62, 1.76, 2.35, and 2.61 Å, respectively, which are consistent with the values reported in the literature [17,18]. From Fig. 2(b), the average CNs of Si–O, Al–O, Ca–O, and O–O were 4.05, 4.39, 5.51, and 6.73, respectively. The results show that the Si–O structure in the melt is more stable than the Al–O structure. The abscissae corresponding to the first valley in the Si–O and Al–O RDF curves were 2.0 and 2.5 Å, respectively, which indicates that O atoms do not exist on the spherical surface within 2.0 and 2.5 Å of the Si and Al atoms, respectively. Thus, the cutoff radii of 2.0 Å for Si–O and 2.5 Å for Al–O were selected in this investigation.

The average coordination function describes the distribution of other particles around the particles, showing the distribution of atoms and structural units. For example, the changes in $N_{Si–Si}(r)$ and $N_{Si–Al}(r)$ in the $CaO–SiO_2–Al_2O_3$ systems with CaO/SiO_2 = 1 (mole ratio) and varying Al_2O_3 content are shown in Fig. 3. An increase in the content of Al_2O_3 from 6 to 34 mol% (CSA1 to CSA8, see Table 2) led to a gradual decrease in $N_{Si–Si}(r)$ from 1.88 to 0.89, whereas $N_{Si–Al}(r)$ increased from 1.02 to 4.11. These results indicate that the formation of the $[AlO_4]^{5-}$ tetrahedron structure hinders the formation of a $[SiO_4]^{4-}$ tetrahedron network structure and the $[AlO_4]^{5-}$ occupy the $[SiO_4]^{4-}$ sites.

3.2. Distribution of oxygen and q^i species

The distribution of oxygen species in the different systems studied at 1600 °C is shown in Fig. 4. The proportion of O_f was small across all systems investigated. As the structure of Ca–O–Ca is unstable, the amount of free O^{2-} was negligible in the $CaO–SiO_2–Al_2O_3$ melt and thus is discussed. As the content of Al_2O_3 increased, the concentration of O_{nb} decreased, and the concentration of O_b and O_t increased. Thus, as the content of Al_2O_3 increased, O_{nb} polymerized to form O_b and O_t. Notably, the concentration of O_b increased to a maximum value when the CaO/Al_2O_3 mole ratio reached 1, at which point, the concentration of O_t increased significantly. In systems with a low alkalinity and a high Al_2O_3 content, there is an insufficiently low number of alkaline metal cations to balance the excess negative charge of the $[AlO_4]^{5-}$tetrahedra, thus, it is believed that the O_t species replace the O_b species to achieve charge balance. This observation is consistent with the results of the spectral study presented therein [19].

The O_b species in the $CaO–SiO_2–Al_2O_3$ system can participate in the following three bonds: Si–O–Al, Si–O–Si, and Al–O–Al. One O atom connects two network-forming nodes T (where T is Si or Al). Fig. 5 shows the distribution of O_b and O_t in the different systems studied. The structural content of Si–O–Al was significantly higher than that of Si–O–Si and Al–O–Al. When the number of Si atoms was higher than the number of Al atoms, the structural content of Si–O–Al increased to a maximum value of ~45% as the concentration of Al_2O_3 increased. This phenomenon conforms to the "Al avoidance principle", that is, the $[AlO_4]^{5-}$tetrahedron structure more easily connects to the $[SiO_4]^{4-}$ tetrahedron structure [20] than the $[AlO_4]^{5-}$ tetrahedron structure, as observed in high SiO_2 systems [4]. In contrast, in the high Al_2O_3 system, Cormier [21] did not find any evidence of the phenomenon wherein the Si–O–Al structure is easier to form than the Si–O–Si or Al-O-Al structure, and the "Al avoidance principle" is not applicable to the high Al_2O_3 systems. Therefore, when the number of Al atoms in the simulation system exceeds the number of Si atoms, the formation likelihood of the Si–O–Al structure gradually decreases and the formation likelihood of the Al–O–Al structure and O_t increases, thus leading to higher proportions of the Al–O–Al structure and O_t.

As shown in Fig. 6, O_t is involved in the following O(Al, Al, Si) and O(Al, Al, Al) structures, where one O atom connects to three T. The content of O(Al, Si,Si) is less than 0.2%, and the content of O(Si, Si, Si) is negligible because the role of O_t is to balance the excess negative charge of the $[AlO_4]^{5-}$tetrahedron structure. As there is no excess charge in the $[SiO_4]^{4-}$tetrahedron structure in the system, Si–O–Si is no longer coordinated to other cations [22]. In the O(Al, Al, Si) and O(Al,

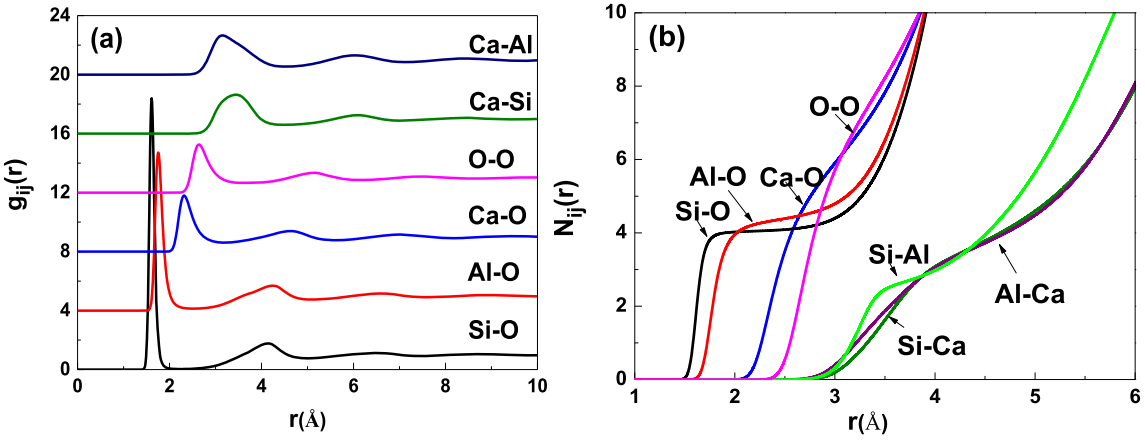

Fig. 2. (a) RDFs and (b) CNs between particles in CSA5.

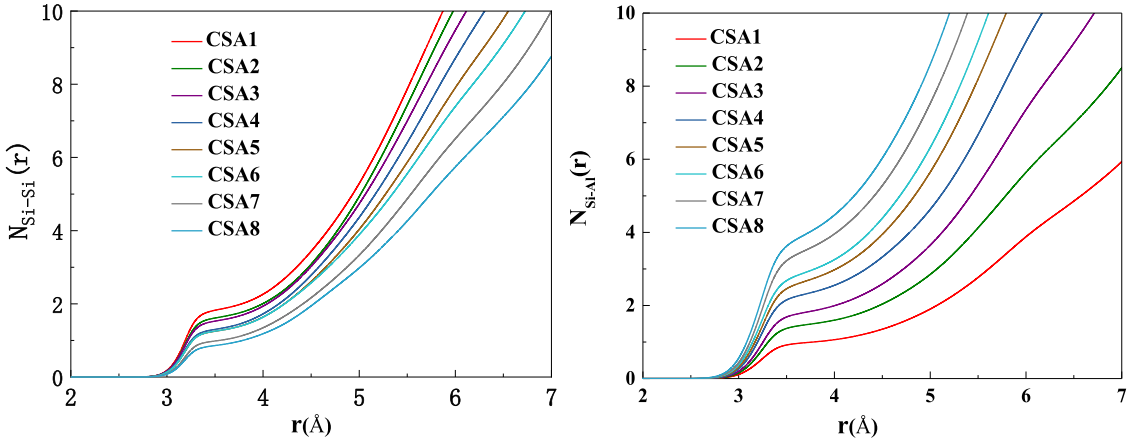

Fig. 3. Distribution of $N_{Si–Si}(r)$ and $N_{Si–Al}(r)$ in the $CaO–SiO_2–Al_2O_3$ systems with $CaO/SiO_2 = 1$ and varying Al_2O_3 content.

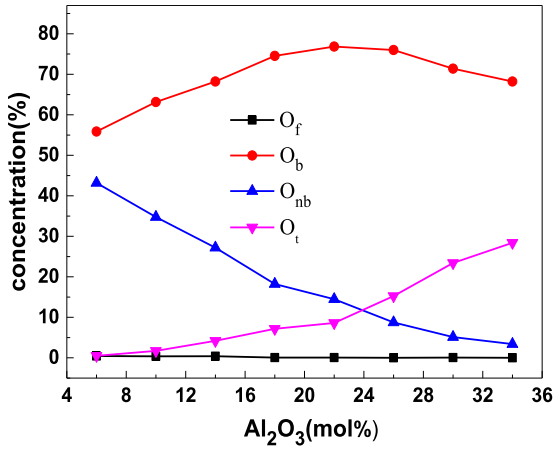

Fig. 4. Distribution of oxygen species in the $CaO–SiO_2–Al_2O_3$ systems of varying Al_2O_3 content and $CaO/SiO_2 = 1$.

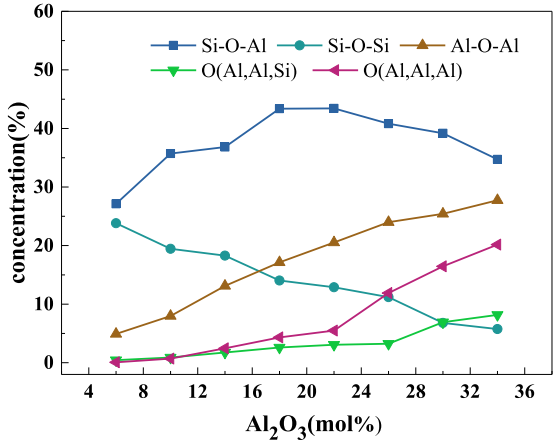

Fig. 5. Distribution of O_b and O_t in the systems studied with different basicity.

Al, Al) structures, the Al–O bond acts as the coordination bond, which balances the charge distribution in the system. Therefore, the charge distribution of O_t and O_b is different as well as the bond energy between the atoms. The structure of O(Al, Al, Al) can be classified as a "common edge" or "non-common edge" structure according to their formation. In the case of the "common edge" structure, two edges from two $[AlO_4]^{5-}$tetrahedra overlap, prompting the release of an O atom. This type of structure formation leads to structural deformation, and an increase in energy and thus increase in structural instability.

Q^i is used to characterize the degree of polymerization and complexity of the melt, and i is refers to the number of O_b of tetrahedral structure. The variation of Q^i with the Al_2O_3 concentration distribution in each system is shown in Fig. 7. As the relative content of Q^0 is less than 0.1%, its distribution is not discussed. As the content of Al_2O_3 increased, Q^4 and Q^5 are formed by the polymerization of Q^3, Q^2, and Q^1. With the further increase of Al_2O_3 content, Q^4 decreased and Q^5 continued to increase. The concentration of Q^5 reached 29.8% when the concentration of Al_2O_3 is 34%. An increase in the proportion of the $[AlO_4]^{5-}$tetrahedron structure makes the system charge more unbalanced. The increase in O_t leads to an increase in the proportion of Q^5 structure, which concurrently makes the system more complex and unstable.

Fig. 8 shows the distribution of the different Al states in the systems as a function of Al_2O_3 concentration. In the $CaO–SiO_2–Al_2O_3$ system, there are four-coordinate, five-coordinate, and six-coordinate Al. With the increase of Al_2O_3 content, the relative content of Al^{IV} decreased, whereas the relative content of Al^{V} increased and the relative content of Al^{VI} remained mostly unchanged. When the CaO/Al_2O_3 is less than 1, an increase in the Al^{V} content was observed mainly due to the insufficient amount of CaO in the system to compensate for the excess negative charge of the $[AlO_4]^{5-}$ tetrahedron structure. This charge imbalance in the coordination system is consistent with changes in the structure of O_t and Q^5 discussed earlier as the Al_2O_3 content increases. This change can be explained by the amphoteric behavior of Al_2O_3. When the level of Ca^{2+} is adequate to compensate for the excess negative charge of the $[AlO_4]^{5-}$tetrahedron structure, Al_2O_3 displays acidity. When the level of the basic cation is insufficient to compensate for the excess negative charge of the $[AlO_4]^{5-}$ tetrahedron structure, a proportion of Al_2O_3 acts as a network modifier to balance the charge and Al_2O_3 shows alkalinity.

3.3. Distribution of bond angles

The distribution of the O–Si-O bond angle under different basicity is shown in Fig. 9(a). The distribution of the O–Si–O bond angle is symmetrical, with a peak centered at about 109°, which is comparable to the theoretical value of a tetrahedral angle of 109.5°. Therefore, it can be confirmed that the Si–O structure in the system is mainly in the form of $[SiO_4]^{4-}$ tetrahedra. For reference, the bond angle of O–Si–O has been determined as 109.47° based on the data model of neutron and high-energy X-ray diffraction [23]. In another investigation [24], the bond angles of SiO_2 and $Na_2Si_2O_5$ have been determined as 109.1° and 109.3°, respectively, based on neutron diffraction analyses. The present calculation is thus consistent with experimental results, thereby demonstrating the reliability of the MD simulation performed in the present research. As shown in Fig. 9(b), the distribution of the O–Al–O

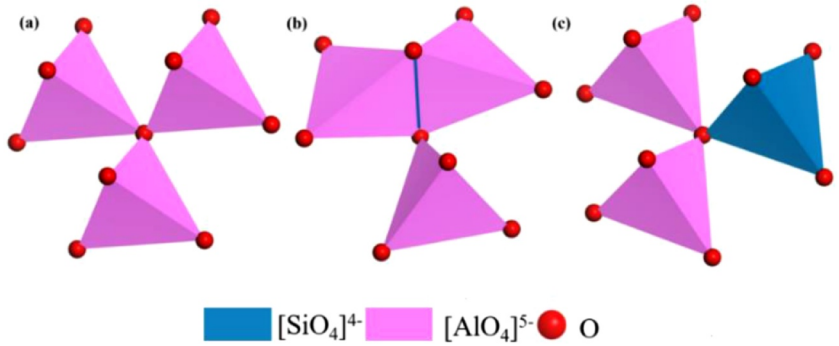

Fig. 6. Equilibrium conformations involving O_t; (a) common edge O(Al, Al, Al); (b) non-common edge O(Al, Al, Al); and (c) O(Al, Si, Si).

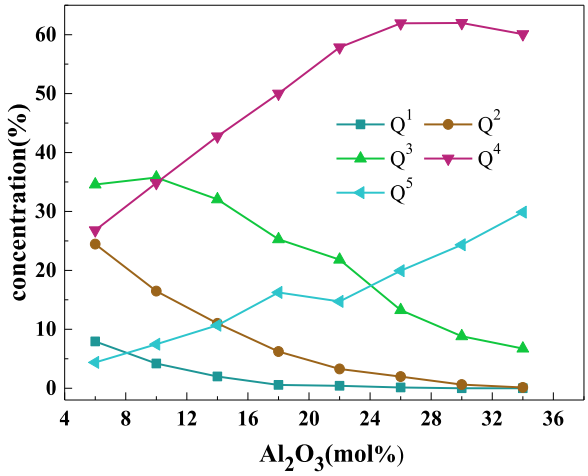

Fig. 7. Distribution of Q^i in the systems studied with different basicity.

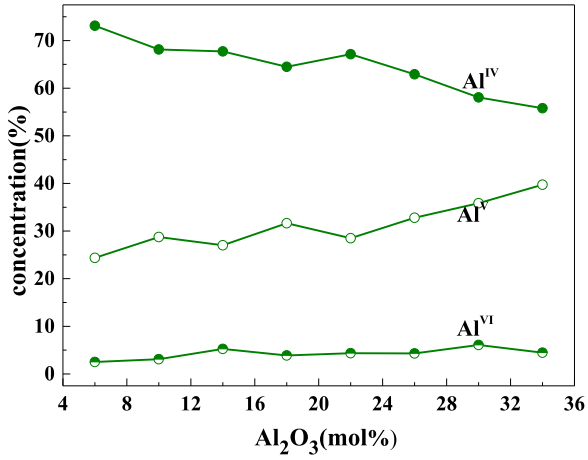

Fig. 8. Distribution of the coordination states of Al under different basicity.

bond angle was symmetrical, with a peak centered at 100–110°. As the concentration of Al_2O_3 increased, the distribution of the O–Al-O bond angle widened, with the peak value shifting to higher degree values. The widened distribution was attributed to the formation of high-coordinate Al in the system and the size of the O–Al–O bond angle is mainly determined by the position of Al in the tetrahedron or octahedron. The extensive bond angle distribution shows that the addition of Al_2O_3 increases the disorder of the system and increases the complexity and instability of the system structure.

4. Structural properties and viscosity

4.1. Self-diffusion coefficients of atoms

According to the Einstein relation, the self-diffusion coefficients of Ca, Si, Al, and O atoms can be obtained from the MSD function, as shown in Fig. 10. The self-diffusion coefficients of the atoms in the systems studied decreased in the order of $D_{Ca} > D_{Al} > D_O > D_{Si}$. The observed trend for D_{Al} and D_O was consistent with the isotope tracing experimental results ($D_{Al} > D_O$) reported by Liang [25] and the simulation results of Tandia [26]. Specifically, herein, D_{Ca} and D_{Si} decreased with increasing Al_2O_3 concentration, whereas D_{Al} and D_O initially decreased with increases in the Al_2O_3 concentration and then increased with further increases in the Al_2O_3. The experimental results showed that the viscosity of the $CaO–SiO_2–Al_2O_3$ system initially increases before decreasing with further increases in the Al_2O_3 concentration at 1873 K [27], which is consistent with the trend observed for D_{Al} and D_O.

As observed from Fig. 10, the value of D_O is similar to that of D_{Si} and D_{Al}, which is between D_{Si} and D_{Al}. In addition, when the concentration of SiO_2 was high, D_O was comparable to D_{Si}, whereas as the Al_2O_3 content increased, D_O was more comparable to D_{Al}.

Therefore, it is assumed that $[SiO_4]^{4-}$ and $[AlO_4]^{5-}$ tetrahedra are the basic structural units of particle diffusion. O atoms move together with Al and Si atoms, as shown in Fig. 11. Similar findings have been reported in other literature [28], but the acid-base changes of Al_2O_3 have no further investigation. D_O depends on the relative concentration of Si and Al. Based on the assumption that the O atom moves in coordination with Si and Al atoms, the self-diffusion of the O atom can be calculated (D_{O*}) according to the D_{Si} and D_{Al} in the same system and the mole percentage of Si and Al atoms as follows [3]:

$$D_{O*} = [Si]\cdot D_{Si} + [Al]\cdot D_{Al} \quad (7)$$

where [Si] and [Al] are the mole percentages of Si and Al atoms respectively, which are expressed as follows:

$$[Si] = x(SiO_2)/(x(SiO_2) + 2x(Al_2O_3)) \quad (8)$$

$$[Al] = 2x(Al_2O_3)/(x(SiO_2) + 2x(Al_2O_3)) \quad (9)$$

Where x is mole fraction.

4.2. Correlation between viscosity and structural properties

The viscosity model database of FactSage software is fitted based on the experimental results of pure oxides and a large number of ternary and binary systems thus the resulting calculated viscosity value is highly accurate [29]. The viscosity of the system with basicity of 0.4 and 1 at 1600 °C was calculated by FactSage software and the Einstein–Stokes formula, as shown in Table 3. The results showed that in the system with basicity 1 ($R = 1$), the viscosity increased with increasing Al_2O_3 concentration up to a maximum value of 0.539 Pa•s

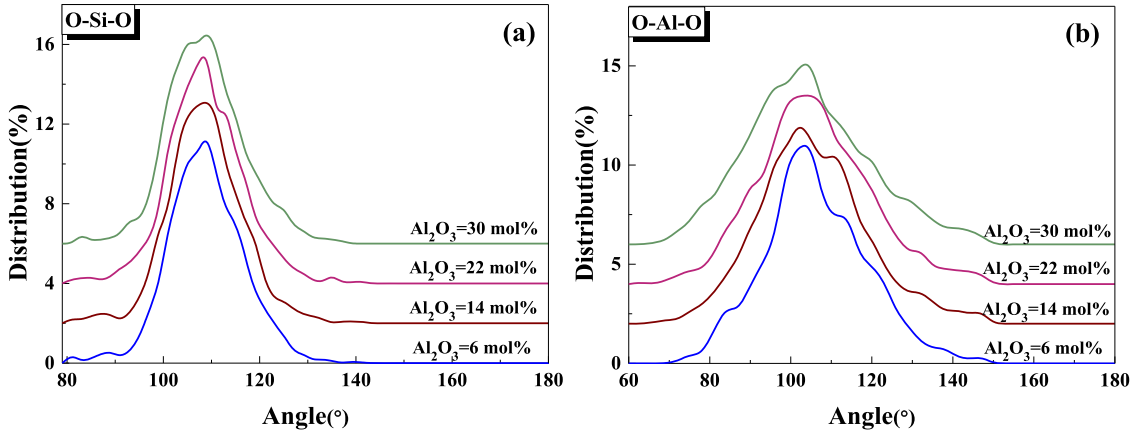

Fig. 9. Distribution profiles of the (a) O–Si–O bond angle and (b) O–Al–O bond angle in the systems.

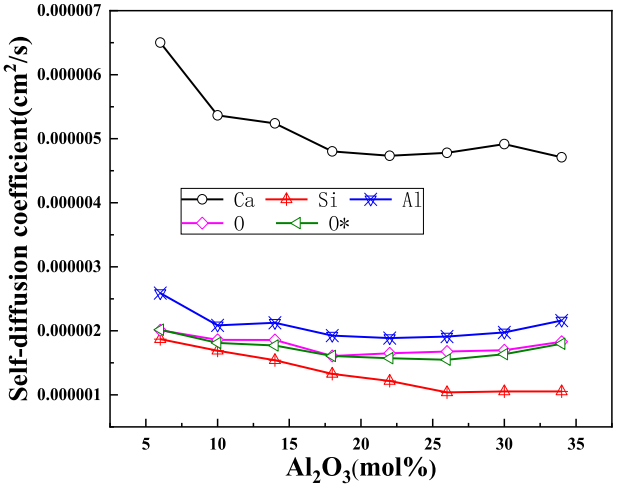

Fig. 10. Self-diffusion coefficients of Ca, Si, Al, and O atoms and calculated O*.

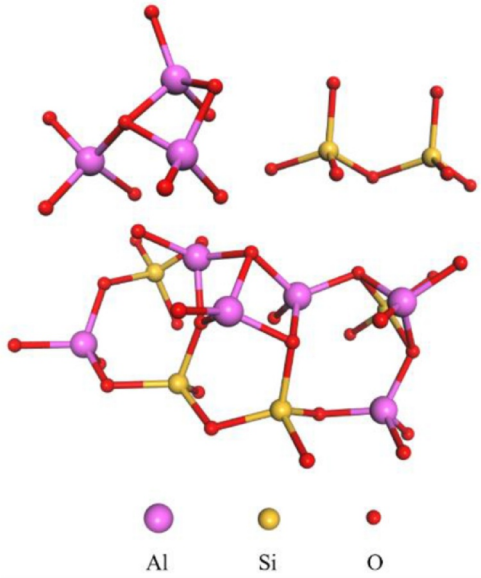

Fig. 11. Schematic of the migration and replacement of partial structural units.

when the Al_2O_3 concentration was 26 mol%, before decreasing gradually with further increases in the Al_2O_3 concentration. Likewise, the MD simulation inferred a maximum value when the Al_2O_3 concentration was 26 mol%. In addition, the liquidus temperature of the system was determined according to the ternary phase diagram of $CaO–SiO_2–Al_2O_3$. At 1600 °C, the superheat of the high Al_2O_3 system decreased, whereas the viscosity decreased. Therefore, variations in the structure led to changes in the rheological properties of the melt. As shown in Fig. 12, the viscosity calculation results of FactSage and MD simulation generated similar trends, indicating that MD simulation can be used to predict the macroscopic properties of slag.

The macro properties of the melt are determined by the microstructure, especially the rheological properties of the melt, which are often related to the complexity of the melt microstructure and the interaction between particles in the system. Changes in O_{nb} and O_t as a function of Al_2O_3 concentration in the system are shown in Fig. 13. As the concentration of Al_2O_3 increased, the O_{nb} content decreased from 42.6 to 3.2%, whereas the proportion of O_t increased from 2.3 to 30.9%. Although the O_{nb} content decreased significantly and the polymerization degree increased, D_O and D_{Al} did not decrease continuously owing to the increase in the polymerization degree in the high Al_2O_3 system, indicating that the self-diffusion coefficient was affected by other factors. When the number of Ca atoms is insufficient to compensate for the excess negative charge of the $[AlO_4]^{5-}$ tetrahedron structure, the amount of O_t increased significantly. When the content of O_t reached 17.8%, D_O increased with an increase in the Al_2O_3 content. The change of the different coordination states of Al as a function of Al_2O_3 concentration is shown in Table 4. Al is mainly tetra-coordinated, and the Al^V content was between 24 and 40%. When the content of Ca atoms was insufficient, the Al^{IV} content decreased and the Al^V increased. In CSA6–CSA8, the diffusion properties of Al and O were influenced by O_t and high-coordinate Al.

The viscosity–temperature curve of the $CaO–SiO_2–Al_2O_3$ system calculated by FactSage is shown in Fig. 14. As the Al_2O_3 content in the ternary system increased, the viscosity increased gradually, which is attributed to the increase in the polymerization degree of the system, as confirmed by the MD simulation results mentioned above. However, with a further increase in the Al_2O_3 content, the viscosity decreased, which is due to the large increase in the O_t and high-coordination Al contents and the reduced stability of the system structure. Neuville [30] has reported that Al^V is a transition state in the viscous flow process of aluminosilicate melts and the Al–O structure in $[AlO_5]$ and $[AlO_6]$ is unstable, resulting in an increase in the diffusion coefficients of Al and O and a decrease in the viscosity of the system. Therefore, the coordination number of Al can be used to characterize the acid–base changes in Al_2O_3. Both $[AlO_5]$ and $[AlO_6]$ have an Al–O ionic bond. Al contributes to charge compensation effects in the system and switches from being a network-forming agent to a network modifier [26].

Mott [31] proposed a method to express the relationship between atomic diffusion and viscous flow and described the viscous flow of melts according to the movement of point defects. The findings have

Table 3
Viscosity of the systems at 1600 °C calculated by molecular dynamics simulation and FactSage.

Al_2O_3 (mol%)		6	10	14	18	22	26	30	34
R = 0.4	$\eta_{FactSage}$ (Pa•s)	3.884	4.658	5.428	5.913	5.831	5.094	3.947	/
	η_{MD} (Pa•s)	4.176	4.876	5.713	6.585	6.021	5.351	4.187	/
R = 1	$\eta_{FactSage}$ (Pa•s)	0.298	0.339	0.406	0.469	0.516	0.539	0.535	0.506
	η_{MD} (Pa•s)	0.458	0.499	0.521	0.574	0.587	0.596	0.564	0.513
	T_{LQ} (°C)	1416	1297	1321	1370	1391	1408	1476	1532

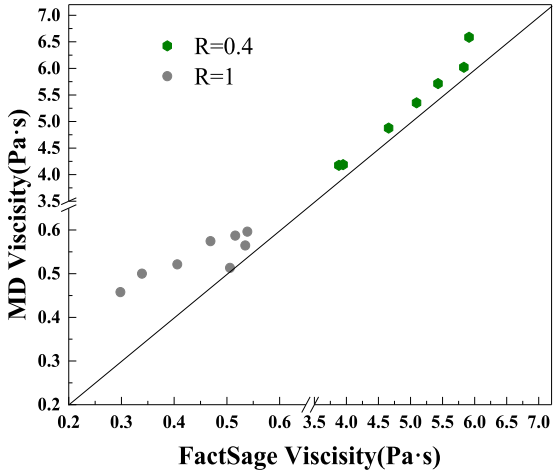

Fig. 12. Comparison of the viscosities of the systems determined by MD simulation and FactSage calculations.

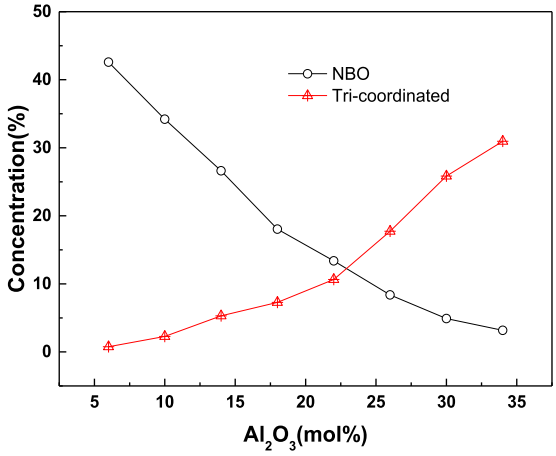

Fig. 13. Effect of Al_2O_3 concentration on the content of O_{nb} and O_t.

Table 4
Changes in the content of the Al coordination states as a function of Al_2O_3 concentration.

Coordination Number	CSA1	CSA2	CSA3	CSA4	CSA5	CSA6	CSA7	CSA8
Al^{IV}	73.12	68.14	67.72	64.5	67.15	62.91	58.06	55.79
Al^{V}	24.37	28.76	27.02	31.64	28.5	32.79	35.84	39.74
Al^{VI}	2.5	3.1	5.26	3.87	4.35	4.3	6.09	4.47

shown that structural defects (defects of oxygen) greatly influence the atomic diffusion and viscous flow of melts. The connection of the third cation to the Al–O–Al structure, forming O_t, disrupts the charge distribution around O and lengthens the Al–O bond, which reduces the stability of the structure, as shown in Fig. 15. Therefore, in the CaO–SiO_2–Al_2O_3 system, the structure parameters D(O/T) were established

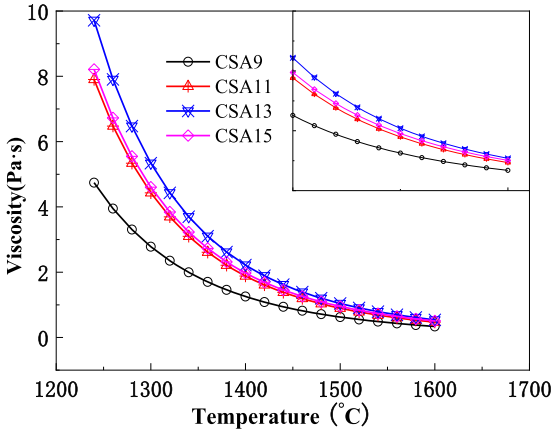

Fig. 14. FactSage calculation changes in the slag viscosity of the ternary system with different Al_2O_3 content as a function of temperature.

by combining the structural defects of O_{nb} and O_t, and the flow properties of the structure were characterized by the ratio of the content of O_{nb} and O_t in the system to the network-forming node T. As shown in Fig. 16, the structural parameter D(O/T) strongly correlated to the natural logarithm of the melt viscosity, which indicates that the diffusion performance of the atom is influenced by the content of O_{nb} and O_t and the viscosity of the system. When there is excess negative charge in the CaO–SiO_2–Al_2O_3 system, the O_t and Al^V content increased significantly. Thus, a proportion of Al_2O_3 releases both O^{2-} and equilibrium charge is adjusted at the same time, thereby reducing the viscosity of the melt.

5. Conclusions

The structures and dynamic properties of CaO–SiO_2–Al_2O_3 melt were studied by MD simulation. Specifically, the effect of the amphoteric nature of Al_2O_3 on the structure and properties of the ternary system were analyzed. The main conclusions are as follows:

(1) The $[SiO_4]^{4-}$ tetrahedron and $[AlO_4]^{5-}$ tetrahedron are the main structural units in the melt. In the high Al_2O_3 systems, there is an insufficiently low amount of Ca^{2+} to compensate for the excess negative charge of the $[AlO_4]^{5-}$tetrahedron structure. The contents of O_t and high-coordinate Al increase significantly.
(2) The self-diffusion coefficient of the atoms in the melt decreases in the order of $D_{Ca} > D_{Al} > D_O > D_{Si}$. The $[SiO_4]^{4-}$tetrahedra and $[AlO_4]^{5-}$ tetrahedra in the system are the basic structural units of particle diffusion and the O atom moves in coordination with Al and Si.
(3) Changes in the acidity and alkalinity of Al_2O_3 depend on the composition of the melt. When the level of the basic cations is sufficiently high, Al_2O_3 is acidic, forming a network structure. When the level of the basic cations is insufficient, a proportion of Al_2O_3 is alkaline, thereby affording O atoms and charge balance.

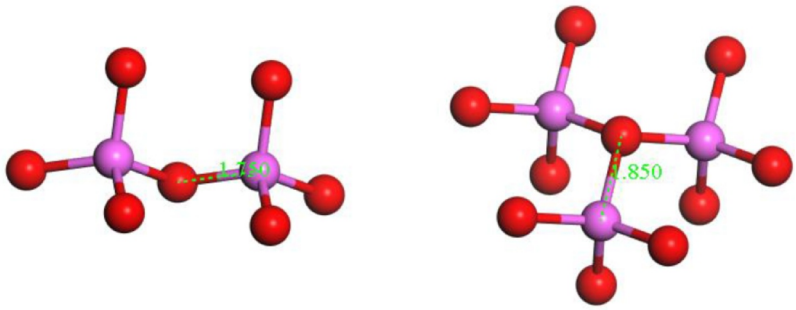

Fig. 15. Schematic showing the Al–O bond length in different structural units. Al and O atoms are colored purple and red, respectively.

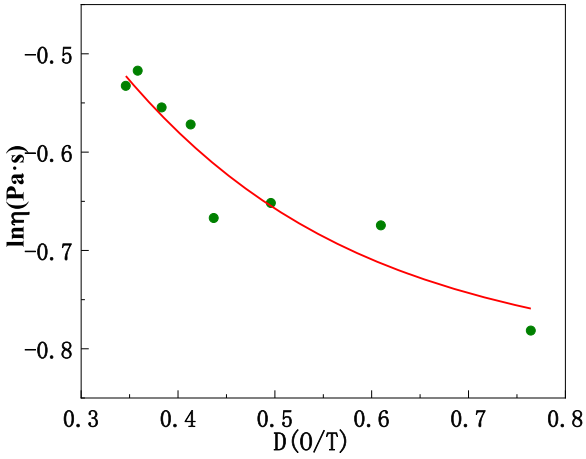

Fig. 16. Relationship between natural logarithm of viscosity and structural parameter D(O/T).

CRediT authorship contribution statement

Yang Chen: Conceptualization, Methodology, Software, Validation, Data curation, Writing - original draft. **Weijie Pan:** Visualization, Investigation. **Boran Jia:** Supervision. **Qiangqiang Wang:** Software, Validation. **Xubin Zhang:** Resources, Data curation. **Qian Wang:** Validation, Supervision. **Shengping He:** Project administration, Writing - review & editing.

Declaration of Competing Interest

The authors declare that they have no known competing financial interests or personal relationships that could have appeared to influence the work reported in this paper.

Acknowledgements

The authors would like to deeply appreciate the fund support from the National Natural Science Foundation of China (project no. 520740547 and project no. 51874057 and 51804057) and the Key projects of national natural science foundation of China (project no. U1660204).

References

[1] Y. Wu, H. Hou, H. Chen, J. You, G. Jiang, Coordination and bond properties of Al and Si ions in system of Al_2O_3-SiO_2 melts, Trans. Nonferrous Met. Soc. China. 11 (2001) 965–971.
[2] Y.Q. W.u, J.L. Y.ou, G.C. J.iang, Molecular dynamics study of the structure of calcium aluminate melts, J. Inorg. Mate. 18 (2003) 965–971.
[3] K. Zheng, F. Yang, X. Wang, Z. Zhang, Investigation of self-diffusion and structure in calcium aluminosilicate slags by molecular dynamics simulation, Mater. Sci. Appl. 2 (2014) 73–80.
[4] K. Zheng, Z. Zhang, F. Yang, S. Sridhar, Molecular dynamics study of the structural properties of calcium aluminosilicate slags with varying Al_2O_3/SiO_2 ratios, ISIJ Int 52 (2012) 342–349.
[5] J.F. Stebbins, I. Farnan, X. Xue, The structure and dynamics of alkali silicate liquids: a view from NMR spectroscopy, Chem. Geol. 96 (1992) 371–385.
[6] K. Hirao, K. Kawamura, Material design using personal computer, Shokabo, Tokyo, 1994, pp. 52–54.
[7] F.D. B.i, F.H. G.e, T.Y. Q.in, Calculation of slag melt density, Tech. Trans. Seri (Chong Qing) 1 (1994) 54–56.
[8] R. Kubo, The fluctuation-dissipation theorem, Rep. prog. Phy. 29 (1996) 255.
[9] N. Shimizu, I. Kushiro, Diffusivity of oxygen in jadeite and diopside melts at high pressures, Geochim, Cosmochim. Acta 48 (1984) 1295–1303.
[10] J.E. M.ungall, Empirical models relating viscosity and tracer diffusion in magmatic silicate melts, Geochim, Cosmochim. Acta 66 (2002) 125–143.
[11] D. Tinker, C.E. L.esher, G.M. B.axter, T. Uchida, Y. Wang, High-pressure viscometry of polymerized silicate melts and limitations of the Eyring equation, Am. Mineral. 89 (2004) 1701–1708.
[12] D. Nevins, F.J. S.pera, M.S. G.hiorso, Shear viscosity and diffusion in liquid $MgSiO_3$: transport properties and implications for terrestrial planet magma oceans, Am. Mineral. 94 (2009) 975–980.
[13] J.E. R.eid, B.T. P.oe, D.C. R.ubie, N. Zotov, M. Wiedenbeck, The self-diffusion of silicon and oxygen in diopside ($CaMgSi_2O_6$) liquid up to 15 GPa, Chem. Geol. 174 (2001) 77–86.
[14] F. J. S.pera, M. S. G.hiorso, D. Nevins, Structure, thermodynamic and transport properties of liquid $MgSiO_3$: comparison of molecular models and laboratory results,75 (2010): 1272–1296.
[15] B.T. Poe, P.F. McMillan, Silicon and oxygen self-diffusivities in silicate liquids measured to 15 gigapascals and 2800 Kelvin, Science 276 (1997) 1245–1248.
[16] T. Schlick, Molecular Modeling And Simulation, Springer-Verlag, New York, 2002.
[17] L. Cormier, D.R. N.euville, G. Calas, Structure and properties of low-silica calcium aluminosilicate glasses, J. Non-Cryst. Solids 274 (2000) 110–114.
[18] P. Ganster, M. Benoit, W. Kob, J.M. Delaye, Structural properties of a calcium aluminosilicate glass from molecular-dynamics simulations: a finite size effects study, J. Chem. Phys. 120 (2004) 10172–10181.
[19] P. Mcmillan, B. Piriou, The structures and vibrational spectra of crystals and glasses in the silica-alumina system, J. Non-Cryst. Solids 53 (1982) 279–298.
[20] W. Loewenstein, The distribution of aluminum in the tetrahedra of silicates and aluminates, Am. Mineral. 39 (1954) 92–96.
[21] L. Cormier, D. Ghaleb, D.R. N.euville, J.M. D.elaye, G. Calas, Chemical dependence of network topology of calcium aluminosilicate glasses: a computer simulation study, J. Non-Cryst. Solids 332 (2003) 255–270.
[22] L.Y. X.u, X.L. W.ang, Y.Q. W.u, G.C. J.iang, Coordination and dynamics of oxygen in calcium aluminosilicate melts, J. Chin. Ceram. Soc. 34 (2006) 1117–1123.
[23] J. Neuefeind, K.D. L.iss, Bond angle distribution in amorphous germania and silica, Beri. Buns. physikalische Chem. 100 (1996) 1341–1349.
[24] M. Misawa, D. Price, K. Suzuki, The short-range structure of alkali disilicate glasses by pulsed neutron total scattering, J. Non-Cryst. Solids 37 (1980) 85–97.
[25] Y. Liang, F.M. R.ichter, A.M. D.avis, E. Bruce Watson, Diffusion in silicate melts: I. Self diffusion in CaO-Al_2O_3-SiO_2 at 1500 °C and 1 GPa, Geochim. Cosmochim. Acta 60 (1996) 4353–4367.
[26] A. Tandia, N.T. T.imofeev, J.C. M.auro, K.D. V.argheese, Defect-mediated self-diffusion in calcium aluminosilicate glasses: a molecular modeling study, J. Non-Cryst. Solids 357 (2011) 1780–1786.
[27] J.H. P.ark, D.J. M.in, H.S. S.ong, Amphoteric behavior of alumina in viscous flow and structure of CaO-SiO_2(-MgO)-Al_2O_3 slags, Metall, Mater. Trans. B 35 (2004) 269–275.
[28] M. Benoit, S. Ispas, Structural properties of molten silicates from ab initio molecular-dynamics simulations: comparison between CaO-Al_2O_3-SiO_2 and SiO_2, Phys. rev. b 64 (2001) 224205.
[29] J.C. v.an Dyk, F. Waanders, S. Benson, M. Laumb, K. Hack, Viscosity predictions of the slag composition of gasified coal, utilizing FactSage equilibrium modelling, Fuel 88 (2009) 67–74.
[30] D. Neuville, L. Cormier, V. Montouillout, D. Massiot, Local Al site distribution in aluminosilicate glasses by 27Al MQMAS NMR, J. Non-Cryst 353 (2007) 180–184.
[31] N. Mott, The viscosity of vitreous silicon dioxide, Philos. Mag. B 56 (1987) 257–262.